Journal of Power Sources 251 (2014) 331–337

Contents lists available at ScienceDirect

Journal of Power Sources

journal homepage: www.elsevier.com/locate/jpowsour

Li_2S-reduced graphene oxide nanocomposites as cathode material for lithium sulfur batteries

Kai Han [a,b], Jingmei Shen [b], Cary M. Hayner [b], Hongqi Ye [a], Mayfair C. Kung [b], Harold H. Kung [b,*]

[a] College of Chemistry and Chemical Engineering, Central South University, Changsha 410083, China
[b] Department of Chemical and Biological Engineering, Northwestern University, Evanston, IL 60208, USA

HIGHLIGHTS

- Li_2S nanoparticles (20–40 nm) in a reduced graphene oxide matrix were synthesized.
- Nano-Li_2S-reduced graphene oxide composite is suitable as cathode material for Li-S batteries.
- Polysulfide additive in the electrolyte facilitates activation of Li_2S particles.

GRAPHICAL ABSTRACT

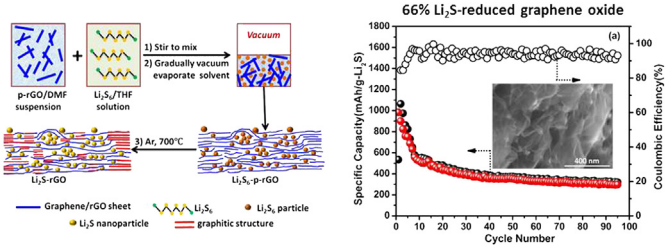

ARTICLE INFO

Article history:
Received 16 August 2013
Received in revised form
30 October 2013
Accepted 21 November 2013
Available online 1 December 2013

Keywords:
Lithium
Sulfide
Battery
Polysulfide
Cathode

ABSTRACT

A lithium sulfide-reduced graphene oxide nanocomposite (Li_2S-rGO) was synthesized and evaluated as the cathode material and Li source for the assembly of Li-S batteries. The composite, with a unique 3-D pocket structure, was synthesized by a combination of facile solution chemistry and thermal treatment. The as-prepared Li_2S-rGO nanocomposites were characterized by X-ray photoelectron spectroscopy, X-ray diffraction and scanning electron microscopy, which showed 20–40 nm Li_2S particles homogeneously dispersed between reduced graphene oxide sheets. Li_2S contents as high as ~66% could be obtained. When used with an electrolyte containing $LiNO_3$ and polysulfide, the Li_2S-rGO nanocomposites exhibited a high initial capacity of 982 mAh g^{-1} Li_2S. However, there was noticeable capacity fade in subsequent cycles, probably due to polysulfide dissolution and the shuttle mechanism, but a capacity of 315 mAh g^{-1} could still be obtained after 100 cycles, with 90–95% coulomb efficiency. The effect of polysulfide additive in the electrolyte on the activation of Li_2S in the first delithiation step was discussed.

1. Introduction

Rapid advances in portable electronics and emerging applications such as electric vehicles, proliferation of wind turbines and solar panels place an ever increasing demand on the energy storage capability of batteries [1–3]. Among future generation of batteries, lithium sulfur batteries are considered one of the most promising [4–6]. The sulfur cathode offers a high theoretical specific capacity of 1672 mAh g^{-1} S or 1166 mAh g^{-1} Li_2S and the energy density of a Li-S battery is up to 2600 Wh kg^{-1}, values that are substantially higher than the present generation of Li ion batteries. In addition, the low cost of sulfur and its environmental friendliness are added attractive features [6,7]. Thus, Li-S batteries have been a subject of intense research.

Most studies on the cycling and rate capabilities of sulfur cathodes employed elemental sulfur as the starting material for cathode and lithium metal for anode. However, such a configuration is not conducive to commercial application, as the use of lithium metal as the lithium source poses manufacturing safety concerns. A much more desirable configuration would be to use

* Corresponding author. Tel.: +1 847 491 7492; fax: +1 847 467 1018.
E-mail address: hkung@northwestern.edu (H.H. Kung).

0378-7753/$ – see front matter © 2013 Elsevier B.V. All rights reserved.
http://dx.doi.org/10.1016/j.jpowsour.2013.11.062

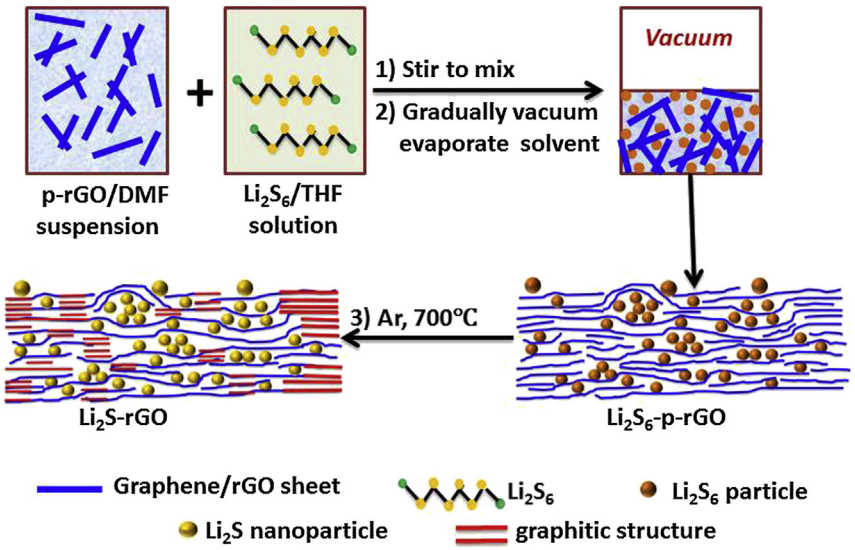

Fig. 1. The synthesis process of Li_2S-rGO composite in which Li_2S nanoparticles are contained in pocket-like structure formed from reduced graphene oxide sheets (not to scale).

Li_2S, the fully discharged state of a Li-S battery, as the starting material for cathode and the Li source. A few recent studies have demonstrated that Li_2S could be used [8–18], and such a cathode material can be coupled with silicon or tin-based anodes [10,12,13].

However, use of Li_2S as the starting cathode material faces technical challenges with synthesis and performance issues beyond those encountered by sulfur. For example, it has been discovered that a large potential barrier (~1 V) in the first charge cycle, so-called activation process, has to be overcome at the beginning of charging when micrometer-sized Li_2S particles (1–10 μm) were used [9,16,17], causing an initial capacity utilization penalty. The origin of this activation process is not well understood. As a basis of our work, we postulated that the problem is due to the poor electrical conductivity of Li_2S, and it can be alleviated by using particles of nanometer dimensions. At present, there is no commonly applied procedure to synthesize Li_2S nanoparticle. In general, any method would have to accommodate the moisture sensitivity and reactivity of lithium sulfide [14]. One published method is to ball-mill commercially available large particles of Li_2S with carbon black [9,16]. Other methods include reacting Li_2SO_4 with carbon at 900 °C, and by reacting PAN, as the precursor for carbon, with Li_2S_3, as precursor for Li_2S, with the aim to promote their binding through interaction between nitrile group and lithium [8,14]. Nevertheless, the synthesis method of integrating nano-sized Li_2S with pre-existed carbon, such as graphene and carbon nanotube, has not yet been reported.

In addition to the synthetic challenges, studies of sulfur cathodes revealed other operational problems, including low coulombic efficiency, poor rate capability and rapid capacity fade. It is understood that the contributing factors of these problems include electrical insulating nature of sulfur and Li_2S, the high solubility and diffusivity of intermediate product polysulfide in the organic electrolyte, and volumetric change upon cycle [19–22]. Various strategies have been attempted to combat these problems by incorporating sulfur into conducting matrices, such as porous carbon [23–25], carbon nanotube [26], graphene [27,28] and conductive polymer [29,30], and storage capacities close to the theoretical capacity have been achieved with engineered structures [31]. Other studies focused on developing electrolytes or additives to prevent dissolution of polysulfide and protect the lithium metal in the anode [32–36].

Here, we report a facile synthesis method to prepare a unique Li_2S-graphene nanocomposite as cathode material, in which nano-size Li_2S particles, formed by thermal decomposition of Li_2S_6 precursor, are entrapped in pocket-like regions in a 3-D reduced graphene oxide network (Fig. 1). Our expectation was that such architecture would support and stabilize nano-size Li_2S particles and enhance their efficient utilization due to the presence of highly conducting and large surface-area reduced graphene oxide sheets that provide excellent electrical contact. The flexibility and mechanical robustness of reduced graphene oxide could help accommodate the volume changes throughout cycling. This solution-based method is easily scalable, and the resulting Li_2S-G nanocomposites were characterized with respect to their microstructure, morphology, Li_2S content, and electrochemical performance. The results of these measurements are reported and discussed, as well as the effect of polysulfide additive in the electrolyte on the initial activation process.

2. Experimental methods

2.1. Synthesis of Li_2S-G nanocomposites

A schematic of the synthesis process is shown in Fig. 1. Graphene oxide (GO) was firstly synthesized from flake graphite using a modified Hummers method, as reported earlier [37]. In brief, the graphite was pre-oxidized by concentrated H_2SO_4, $K_2S_2O_8$ and P_2O_5 and oxidized deeply by concentrated H_2SO_4 and $KMnO_4$. Following centrifugation and washing, a homogeneous aqueous GO dispersion was obtained by ultrasonication. In order to make this suspension compatible with the nonaqueous solution of Li polysulfide used later in the preparation, the GO was partially reduced by mixing in hydrazine monohydrate at 95 °C for 1 h. The mass ratio of N_2H_4 to GO was controlled at 7:10. After centrifugation, washing and vacuum drying at 80 °C overnight, a black, partially reduced graphene oxide (p-rGO) powder was obtained. Typically, 23 mg of p-rGO powder was then dispersed in 5 ml DMF (dimethylformamide) with the aid of ultrasonication for at least 1 h to form a stable suspension.

For the preparation of the Li_2S_6-rGO precursor, 46 mg Li_2S (Alfa Aesar) powder was stirred with 160 mg sulfur in 20 ml of THF (anhydrous) at 50 °C for 20 h under an argon atmosphere to form a

Li_2S_6 solution. The formation of Li_2S_6 was confirmed by UV–Visible absorption spectroscopy (Fig. S1 in supporting information). The p-rGO suspension was then added to the Li_2S_6 solution at a mass ratio of 1:2 p-rGO to Li_2S, which would be the Li_2S content in the final product. After vigorously stirring for at least 2 h, the mixture was gradually vacuum evaporated at 80 °C to remove all the liquid. The resulting solid black powder was removed from the flask wall, ground into a fine powder in an argon glove box, and labeled Li_2S_6-p-rGO. The Li_2S-rGO nanocomposites were finally obtained by thermal treatment of Li_2S_6-p-rGO at 700 °C for 1 h in a flow of argon (100 ml min^{-1}) in a quartz tube. Since Li_2S and Li_2S_6 are both moisture sensitive, all experiments were carried out under an argon atmosphere.

2.2. Material characterization

X-ray diffraction (XRD) patterns of Li_2S_6-p-rGO precursor and Li_2S-rGO nanocomposite were collected with a Scintag XDS2000 diffractometer (Cu Kα, $\lambda = 1.5418$ Å). The morphologies of the as-prepared nanocomposites were examined using a Hitachi S-4800 field emission scanning electron microscopy (FE-SEM) with an energy dispersive spectroscopy (EDS) detector. Thermogravimetric analysis (TGA) was performed with TGA/SDTA851e analyzer (Mettler Toledo) in N_2 below 300 °C and air from 300 to 800 °C. X-ray photoelectron spectroscopy (XPS) was conducted using Thermo Scientific ESCALAB 250Xi equipped with an electron flood gun and a scanning ion gun, and using Al Kα radiation (1486.6 eV) as the excitation source. UV–Vis absorption spectra were obtained using a Perkin Elmer LAMBDA 1050 spectrophotometer.

2.3. Electrochemical measurements

Electrochemical measurements were conducted using CR2032 coin cells with lithium metal as the counter electrode at room temperature. The cathode was prepared by mixing Li_2S-rGO nanocomposites (80 wt.%), Super P (10 wt.%) and PVDF binder (10 wt.%) in a *N*-methylpyrrolidone (NMP) solution. The slurry was then coated onto an Al foil (0.025 mm thick, Alfa Aesar) current collector and vacuum dried at 110 °C for 8 h. A typical mass loading of Li_2S active material in the cathode was ~0.96 mg cm^{-2}. The electrolyte was 1.0 M lithium bis(trifluoromethanesulfonyl)imide (LITFSI) in 1,3-dioxolane (DOL) and 1,2-dimethoxyethane (DME) at 1:1 volume ratio. Unless specified, 0.2 M $LiNO_3$ and 0.1 M Li_2S_6 polysulfide were added as additives. The Li_2S_6 polysulfide additive solution was prepared by stirring purchased Li_2S and sulfur powders in DOL/DME (1:1) at 50 °C for 6 h. Electrode and electrolyte preparation and cell assembly were all carried out inside an argon glove box with O_2 and H_2O concentrations below 0.1 ppm. Galvanostatic measurements were performed with a BT2000 Potentiostat/Galvanostat system (Arbin Instruments) at various current densities in the voltage range of 1.6–3.5 V vs Li/Li^+ for rate and cycling test. All C rates are based on the theoretical capacity of Li_2S (1 C = 1166 mA g^{-1}).

3. Results and discussion

Fig. 2 shows the XRD patterns of the as-prepared Li_2S_6-rGO precursor and Li_2S-G nanocomposites. A very broad hump around $2\theta = 26°$ in the Li_2S_6-rGO composite indicated the presence of randomly oriented, small domains of graphite formed by the reduction of graphene oxide by hydrazine. There were no peaks attributable to Li_2S_6, suggesting that the polysulfide was X-ray amorphous, consistent with the previous report on Li_2S_3 polysulfide [14]. Li_2S peaks (JCPDS card no. 23-0369) were clearly observable in the XRD pattern after heating the composite to

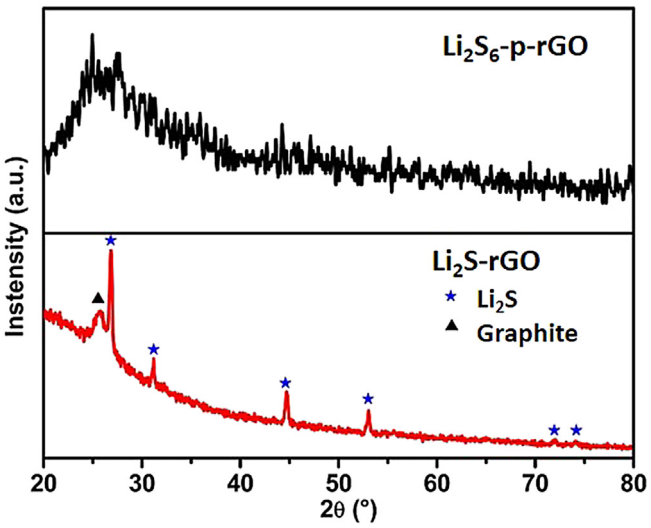

Fig. 2. X-ray diffraction patterns of (top) Li_2S_6-p-rGO and (bottom) Li_2S-rGO nanocomposites.

700 °C, indicating the decomposition of Li_2S_6 to Li_2S (Fig. 2). The formation of Li_2S-rGO composites in which Li_2S was imbedded between graphitic sheets was suggested by the sharpening of the graphite peak at $2\theta = 26°$ after thermal treatment. But the peak remained broad, indicating that although increased restacking of graphenic regions to form domains of graphite had occurred, the domains remained limited in size and density.

A top-view SEM image of Li_2S_6-p-rGO precursor composite is shown in Fig. 3a. Li_2S_6 particles (~100 nm) were detected deposited on the external surface of the composite after evaporation of the solvent. For comparison, Li_2S_6 particles formed by drying in the absence of rGO were much larger, close to μm in dimension. The composite had a sandwich-like structure, as shown by the cross-sectional image in Fig. 3b. There were significant morphology changes after thermal treatment, as shown by images in Fig. 3c–e. First, sharper images of crumpled sheets of rGO sheets were detected after reduction at the high temperature, most likely due to improved electrical conductivity of the composite. Second, 20–40 nm Li_2S nanoparticles, highlighted in Fig. 3d, were discernible as small spheres. The images in Fig. 3d and e suggested that most of the nanoparticles were rather homogeneous distributed underneath the graphene sheets as there were no obvious, large bulges. The decrease in particle size was expected due to loss of sulfur during the decomposition of Li_2S_6 polysulfide to Li_2S. The homogeneous distribution of Li_2S nanoparticles was confirmed by energy dispersive spectroscopy (EDS) line scans for sulfur and carbon elements, shown in Fig. 3f, which showed uniform distributions along the scan line within the spatial resolution of the instrument.

The Li_2S content in the Li_2S-rGO nanocomposites was evaluated from weight increases when Li_2S was oxidized by dry air in the thermogravimetric analysis (TGA). In this analysis, a sample was first purged with N_2 until the temperature reached 300 °C to avoid reaction of Li_2S with residual moisture. Then the gas was switched to dry air and heating continued to 800 °C. As shown in the top panel of Fig. 4, after switching to dry air, the sample increased in weight and its temperature rose faster than the set temperature ramp, indicating that an exothermic event had occurred. After a weight gain of about 40%, this event was complete, and the sample temperature dropped to follow the set temperature ramp. Afterward, the weight gain continued until ~410 °C. In the absence of Li_2S, combustion of graphene was shown to take place between 550 and 650 °C (bottom panel). The Li_2S-rGO data can be explained as

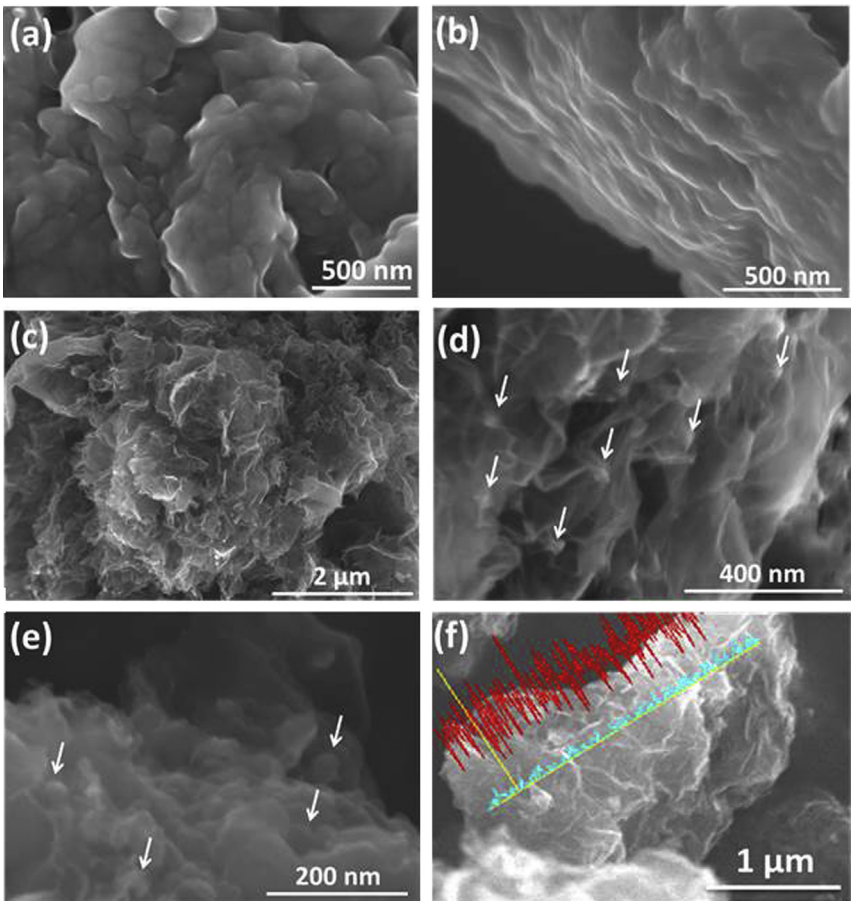

Fig. 3. SEM images of: (a and b) Li_2S_6-p-rGO, and (c, d, and e) Li_2S-rGO nanocomposites. (a) Top surface of Li_2S_6-p-rGO. (b) Cross-section of Li_2S_6-p-rGO. (c, d, and e) Top surface of Li_2S-rGO nanocomposites at three different magnifications. In (d), Li_2S nanoparticles underneath a graphene sheet are highlighted by yellow circles. (f) A line scan electron dispersive spectrum for carbon (red) and sulfur (blue) of Li_2S-rGO nanocomposites (For interpretation of the references to colour in this figure legend, the reader is referred to the web version of this article.).

follows. The rapid weight gain and heat release after switching to air were due to oxidation of the near surface region of the Li_2S nanoparticles to Li_2SO_4 ($Li_2S + 2O_2 \rightarrow Li_2SO_4$). Subsequent weight gain as the temperature continued to ramp up was due to continued oxidation until the entire particle was oxidized at around 500 °C. The final weight change at 800 °C was the sum of weight loss due to the combustion of graphene and weight gain due to oxidation of Li_2S. From these data, the Li_2S content of the sample could be calculated to be ~66%, which was consistent with the proportions of initial material used in its preparation. The formation of Li_2SO_4 in the TGA experiment was confirmed by XRD (JCPDS card no. 20-0640, Fig. S2).

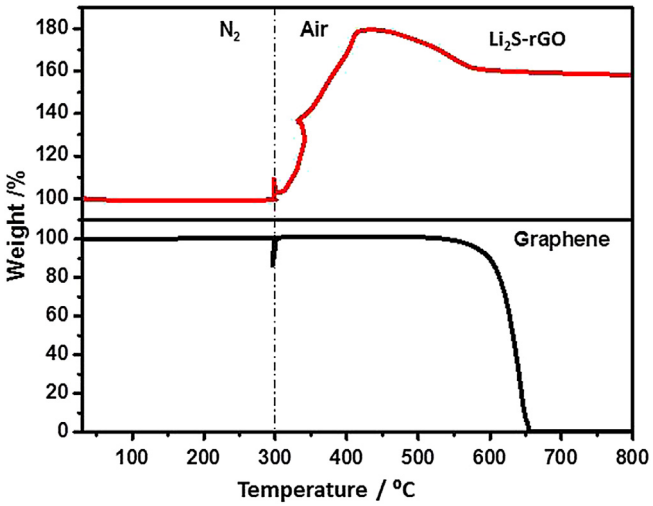

Fig. 4. TGA analysis curves of Li_2S-rGO nanocomposites and pure graphene.

Samples of other Li_2S contents were also prepared by changing the amount of rGO in the preparation suspension. However, large aggregates of Li_2S particles were observed in samples with higher Li_2S contents. Thus, the ~66 wt.% Li_2S was chosen for high capacity without much Li_2S aggregation.

Fig. 5 illustrates the XPS C1s (**5a**) and S2p (**5b**) spectra of Li_2S_6-p-rGO and Li_2S-rGO nanocomposites. Results of curve fitting showed that the majority of carbon existed as sp^2 C (at 284.8 eV) bonded to each other as in graphene. There was residual oxygen in both samples (see also Fig. S3a), and the amount was smaller for Li_2S-rGO. Thus, the GO was effectively reduced to p-rGO by hydrazine in the initial step, and thermal treatment at 700 °C reduced the sample further. The S2p peak for Li_2S_6-p-rGO could be fitted with three peaks at 162.2, 163.4 and 167.4 eV, which could be assigned to S–Li, S–S in Li_2S_6 and SO_3 groups, respectively [21]. After thermal treatment, the major peaks were shifted to 159.8 and 161.7 eV corresponding to the S2p doublet in Li_2S, confirming the decomposition of Li_2S_6. In addition, a new low energy peak appeared at

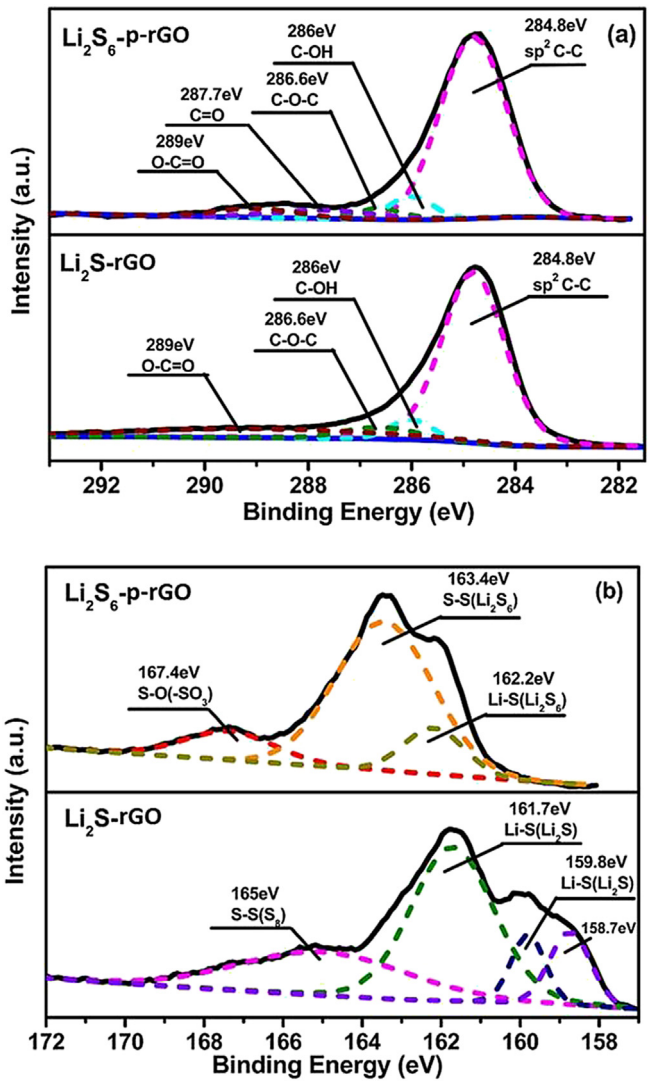

Fig. 5. (a) XPS C1s, and (b) S2p spectra of Li_2S_6-p-rGO and Li_2S-rGO nanocomposites.

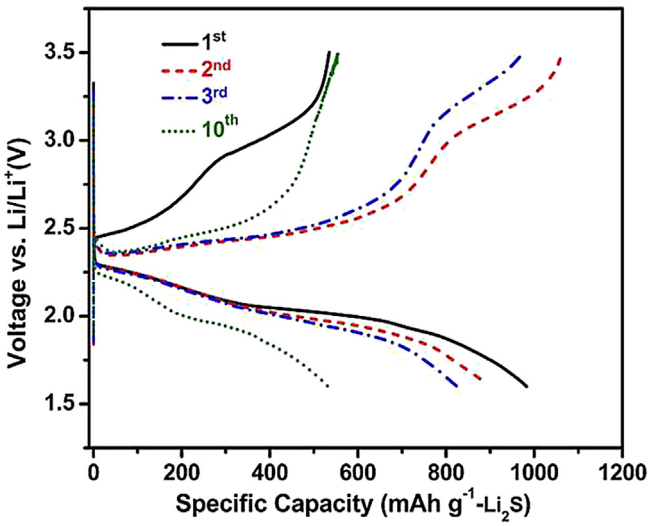

Fig. 6. The discharge/charge voltage profiles between 1.6 and 3.5 V at C/10 rate of the Li_2S-rGO cathode.

158.7 eV, which, based on the low binding energy, we suggested to be from Li_2S interacting strongly with the electron donating graphene support. There was also a low-intensity peak at 165 eV, which indicated the presence of a trace amount of elemental sulfur that was probably formed by condensation of residual sulfur vapor left in the thermal treatment reactor during the cool down process. The presence of lithium in both materials was also confirmed by the Li1s peak centered at 55.5 eV (Fig. S3b).

Fig. 6 displays the initial charge/discharge voltage curves of the lithium sulfur battery with the Li_2S-rGO nanocomposites cathode and Li_2S_6 additive in the electrolyte. The cell was cycled at a constant current of C/10 (i.e., 116 mA g^{-1}) in the voltage window from 1.6 to 3.5 V. The profile of the first delithiation (charging) process showed two sloping plateaus at 2.4–2.6 V and 2.8–3.0 V. The first plateau corresponded to the gradual conversion of Li_2S to Li polysulfide and then to sulfur, and we attributed the second one to the activation of Li_2S particles. In this first delithiation, the electrode material delivered a specific capacity of 534 mAh g^{-1} Li_2S. Two features of the first delithiation voltage profiles should be mentioned. First, a significant portion of the Li_2S could be delithiated without any significant potential barrier in the first charge process, which is different from some literature data for micron-size Li_2S particles in a carbon composite [9,16]. We attributed this to the small size of Li_2S nanoparticles. Smaller Li_2S particles have a larger fraction of material in the near surface region that is more accessible and thus easier to be activated than the material buried in the interior of the particle. In the presence of polysulfide additive, the Li_2S in the near surface region is converted to the more reactive/soluble polysulfide, thus enabling delithiation immediately. It has been demonstrated that the polysulfide additive in the electrolyte could reduce the potential barrier during the first delithiation [8,9].

Second, the sloping plateau at 2.8–3.0 V became smaller with cycling, and eventually disappeared after ten cycles. We interpret this to indicate that by the tenth cycle, there were no more crystalline Li_2S in the sample. That is, the lithiation process does not generate large particles of crystalline Li_2S. Instead, the Li_2S formed was mostly amorphous and/or in the form of very small particles that would not exhibit the high-voltage activation.

Whereas the first delithiation showed a charge capacity of 534 mAh g^{-1} Li_2S, subsequent lithiation showed a much higher capacity of 982 mAh g^{-1} Li_2S. Such a large increase in charge capacity is uncommon. We believe that this is due to the pocket-like morphology of our graphenic electrode material and activation of Li_2S by reaction with polysulfide. As prepared, Li_2S nanoparticles are dispersed in pockets between reduced GO sheets. These pockets are not completely closed, but are accessible to the electrolyte solution via gaps between sheets. After cell assembly, the polysulfide in the electrolyte in these pockets reacts with the surface of the Li_2S particles to form surface polysulfide that is much more electrochemically active than Li_2S. This reaction is well known that long chain polysulfide ($n > 4$) reacts with Li_2S to produce short chain, soluble polysulfide ($n < 4$) in the organic electrolyte solvent [38,39]. We have confirmed this in our laboratory. We observed that by dispersing a Li_2S-rGO sample in a solution of Li polysulfide overnight, there were no more Li_2S diffraction peaks in XRD. However, this reaction is slow in a packaged cell at room temperature because of slow diffusion of polysulfide. Thus, even for the nano-size particles in our samples, only the surface fraction of the Li_2S particle has reacted after one days in the assembled cell. This is the portion that contributed to the observed charge capacity in the first delithiation process. Because of the pocket-like morphology of our material, most of the sulfur that is formed remains in the pocket. Their presence facilitates the continued transformation of the remaining Li_2S to polysulfide. As more polysulfide is formed, some

of it is lost by diffusion into the electrolyte. The overall effect of this chemical transformation process is the loss of Li ions and sulfide ions from the Li_2S cathode to the electrolyte and transfer of elemental sulfur from the electrolyte to the cathode. We propose that the net effect after the first delithiation is a net transfer of sulfur into the pockets of the cathode due to significant conversion of the remaining Li_2S to polysulfide, which results in a higher lithiation capacity than the capacity of the first delithiation.

The lithiation process of our cathode material is similar to those reported in the literature [11,14]. Two voltage plateaus were observed, although they were more sloping than those reported, which could be attributed to polarization phenomena associated with high surface area materials [40,41]. This polarization phenomenon persisted in subsequent cycles while the charge capacity decreased.

Fig. 7a shows the derivative d*Q*/d*V* of the lithiation/delithiation curves of Fig. 6. For the first three cycles, two peaks were apparent during the delithiation process. A peak at 2.45–2.5 V that appeared in every cycle corresponded to the on-set of oxidation of polysulfide to sulfur. Another peak appeared at 2.95 V in the first cycle and was shifted to higher voltages of 3.10 V and 3.25 V in the second and third delithiation cycle, respectively. We attribute this to the oxidation of Li_2S that might not be easily accessible to the electrolyte, such as in the core of a larger Li_2S particle or being trapped in the interior of the graphenic structure. With each cycle, some more of the Li_2S was converted to polysulfide and participated in the electrochemical process until, eventually at tenth cycle or earlier, there was no more of such Li_2S remaining, and this high voltage peak disappeared. The two peaks in the lithiation branch of these curves, at about 2.25 V and 2 V could be assigned to the reduction of sulfur and polysulfide, respectively [4,42].

In the model of the operation described above, the polysulfide in the electrolyte plays an important role in the activation of Li_2S particles. This can be tested by measuring the behavior of the cathode material using an electrolyte without polysulfide. It was found that the accessible charge capacity was quite low (20–50 mAh g^{-1} Li_2S) in the first cycle (Fig. S4). Thus, much less Li_2S was activated. The derivative d*Q*/d*V* curves of the charge/discharge curves shown in Fig. 7b showed that in the first cycle, there was little delithiation until 3.5 V, suggesting that the activation process was more difficult in the absence of polysulfide in the electrolyte. The lithiation branch showed two peaks at 2.1 V and 2.4 V, which were typical for sulfur cathodes. The delithiation curve in cycles 2 and 3 showed delithiation beginning at around 2.3 V, but the charge capacity remained low at ~50 mAh g^{-1} Li_2S, and the high voltage activation peak remained. In addition, there was a large negative peak that began at ~1.7 V, which has been ascribed to the decomposition of $LiNO_3$ additive at the anode [33]. It is interesting that this was not observed in the cell with polysulfide additive. A possible reason is that polysulfide additive in the electrolyte

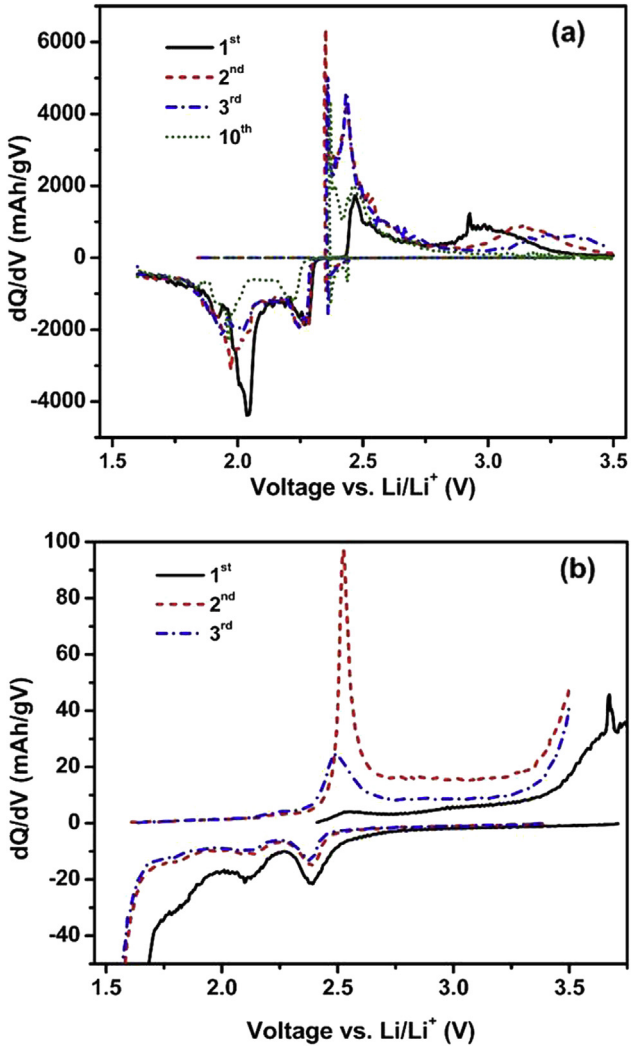

Fig. 7. d*Q*/d*V* curves of Li_2S-rGO cathode with (a) and without (b) polysulfide additive in electrolyte.

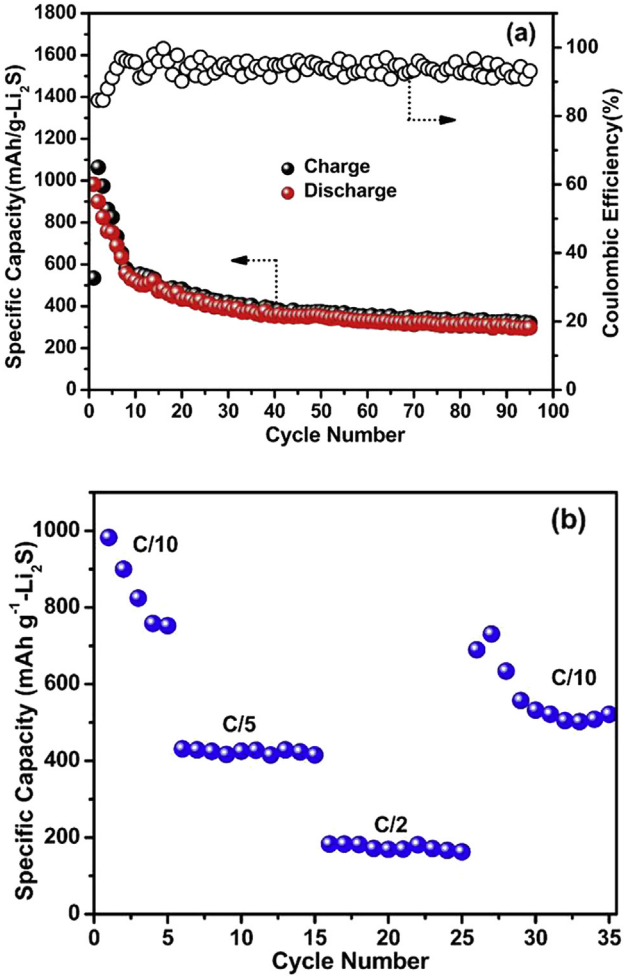

Fig. 8. (a) Cycling performance of Li_2S-rGO nanocomposites at C/10. (b) Rate capability of Li_2S-rGO nanocomposites.

reacted with the lithium metal anode to form a passivation film on the lithium surface that prevented the decomposition of $LiNO_3$ at the anode [34,43].

Finally, prolonged cycling performance was evaluated and the results are shown in Fig. 8a. At a rate of C/10, the lithiation (discharge) capacity of Li_2S-rGO dropped from an initial high of 982 mAh g^{-1} Li_2S rather rapidly to 522 mAh g^{-1} in ten cycles, and then more slowly afterward to 315 mAh g^{-1} after 100 cycles. The coulombic efficiency was between 90 and 95%. The high initial capacity was among the best reported values, although some others reported slower capacity fade [8–11,15–18]. In the literature, the capacity loss has been attributed to dissolution of lithium polysulfide from the cathode into the electrolyte and the shuttling of polysulfide between electrode [22,44]. The charge capability at different C rates is shown in Fig. 8b. After the initial capacity loss, a relatively stable capacity of 425 mAh g^{-1} was obtained with C/5, which dropped to 183 mAh g^{-1} at C/2.

4. Conclusion

A facile, solution chemistry method to synthesize nano-sized Li_2S particles embedded in Li_2S-reduced graphene oxide composite was developed successfully. The composite consisted of 20–40 nm Li_2S particles uniformly dispersed in the pocket-like regions between reduced graphene oxide sheets. The method of depositing Li_2S nanoparticles could be easily extended to other pre-existing carbonaceous matrices, such as carbon nanotube and porous carbon. When used with an electrolyte that contained Li polysufide, the Li_2S-rGO nanocomposites can be used as a Li source immediately, although cycling a few times is needed in order to activate all the Li_2S particles. However, this reduced graphene oxide structure did not resolve the issue of capacity fade, and additional research is needed to overcome this limitation.

Acknowledgments

This research was financed by the U.S. Department of Energy, Basic Energy Sciences, grant DE-AC02-06CH11357 through the Center for Electrical Energy Storage, an Energy Frontier Research Center. This work made use of the J.B. Cohen X-Ray Diffraction Facility at the Materials Research Center, the SEM and XPS in the EPIC and KECK-II facility of NUANCE Center at Northwestern University. Kai Han was supported by China Scholarship Council and Hunan Provincial Innovation Foundation for Postgraduate. Prof. Hongqi Ye was supported by National Natural Science Foundation of China (21276284).

Appendix A. Supplementary data

Supplementary data related to this article can be found at http://dx.doi.org/10.1016/j.jpowsour.2013.11.062.

References

[1] J.B. Goodenough, Y. Kim, Chem. Mater. 22 (2009) 587–603.
[2] J.-M. Tarascon, M. Armand, Nature 414 (2001) 359–367.
[3] B. Scrosati, J. Garche, J. Power Sources 195 (2010) 2419–2430.
[4] X. Ji, L.F. Nazar, J. Mater. Chem. 20 (2010) 9821–9826.
[5] P.G. Bruce, S.A. Freunberger, L.J. Hardwick, J.-M. Tarascon, Nat. Mater. 11 (2011) 19–29.
[6] Y. Yang, G. Zheng, Y. Cui, Chem. Soc. Rev. 42 (2013) 3018–3032.
[7] S.S. Zhang, J. Power Sources 231 (2013) 153–162.
[8] Z. Yang, J. Guo, S.K. Das, Y. Yu, Z. Zhou, H.D. Abruña, L.A. Archer, J. Mater. Chem. A 1 (2013) 1433–1440.
[9] Y. Yang, G. Zheng, S. Misra, J. Nelson, M.F. Toney, Y. Cui, J. Am. Chem. Soc. 134 (2012) 15387–15394.
[10] Y. Yang, M.T. McDowell, A. Jackson, J.J. Cha, S.S. Hong, Y. Cui, Nano Lett. 10 (2010) 1486–1491.
[11] S. Jeong, D. Bresser, D. Buchholz, M. Winter, S. Passerini, J. Power Sources 235 (2013) 220–225.
[12] J. Hassoun, Y.-K. Sun, B. Scrosati, J. Power Sources 196 (2011) 343–348.
[13] J. Hassoun, B. Scrosati, Angew. Chem. Int. Ed. 49 (2010) 2371–2374.
[14] J. Guo, Z. Yang, Y. Yu, H.D. Abruna, L.A. Archer, J. Am. Chem. Soc. 135 (2013) 763–767.
[15] Z.W. Seh, Q. Zhang, W. Li, G. Zheng, H. Yao, Y. Cui, Chem. Sci. 4 (2013) 3673–3677.
[16] K. Cai, M.K. Song, E.J. Cairns, Y. Zhang, Nano Lett. 12 (2012) 6474–6479.
[17] Y. Fu, Y.-S. Su, A. Manthiram, Adv. Energy Mater. (2013), http://dx.doi.org/10.1002/aenm.201300655.
[18] T. Takeuchi, H. Kageyama, K. Nakanishi, M. Tabuchi, H. Sakaebe, T. Ohta, H. Senoh, T. Sakai, K. Tatsumia, J. Electrochem. Soc. 157 (2010) A1196–A1201.
[19] N.S. Choi, Z. Chen, S.A. Freunberger, X. Ji, Y.K. Sun, K. Amine, G. Yushin, L.F. Nazar, J. Cho, P.G. Bruce, Angew. Chem. Int. Ed. Engl. 51 (2012) 9994–10024.
[20] S. Evers, L.F. Nazar, Acc. Chem. Res. 46 (2013) 1135–1143.
[21] Y. Diao, K. Xie, S. Xiong, X. Hong, J. Electrochem. Soc. 159 (2012) A1816–A1821.
[22] Y.V. Mikhaylik, J.R. Akridge, J. Electrochem. Soc. 151 (2004) A1969–A1976.
[23] X. Ji, K.T. Lee, L.F. Nazar, Nat.Mat. 8 (2009) 500–506.
[24] J. Schuster, G. He, B. Mandlmeier, T. Yim, K.T. Lee, T. Bein, L.F. Nazar, Angew. Chem. Int. Ed. 51 (2012) 3591–3595.
[25] B. Zhang, X. Qin, G. Li, X. Gao, Energy Environ. Sci. 3 (2010) 1531–1537.
[26] J. Guo, Y. Xu, C. Wang, Nano Lett. 11 (2011) 4288–4294.
[27] L. Ji, M. Rao, H. Zheng, L. Zhang, Y. Li, W. Duan, J. Guo, E.J. Cairns, Y. Zhang, J. Am. Chem. Soc. 133 (2011) 18522–18525.
[28] H. Wang, Y. Yang, Y. Liang, J.T. Robinson, Y. Li, A. Jackson, Y. Cui, H. Dai, Nano Lett. 11 (2011) 2644–2647.
[29] Y. Fu, A. Manthiram, J. Phys. Chem. C 116 (2012) 8910–8915.
[30] Y. Yang, G. Yu, J.J. Cha, H. Wu, M. Vosgueritchian, Y. Yao, Z. Bao, Y. Cui, ACS Nano 5 (2011) 9187–9193.
[31] G. Zheng, Y. Yang, J.J. Cha, S.S. Hong, Y. Cui, Nano Lett. 11 (2011) 4462–4467.
[32] H.-S. Ryu, H.-J. Ahn, K.-W. Kim, J.-H. Ahn, K.-K. Cho, T.-H. Nam, J.-U. Kim, G.-B. Cho, J. Power Sources 163 (2006) 201–206.
[33] S.S. Zhang, Electrochim. Acta 70 (2012) 344–348.
[34] R. Xu, I. Belharouak, J. Li, X. Zhang, I. Bloom, J. Bareño, Adv. Energy Mater. 3 (2013) 833–838.
[35] S.S. Zhang, J.A. Read, J. Power Sources 200 (2012) 77–82.
[36] W. Weng, V.G. Pol, K. Amine, Adv. Mater. 25 (2013) 1608–1615.
[37] X. Zhao, C.M. Hayner, M.C. Kung, H.H. Kung, Adv. Energy Mater. 1 (2011) 1079–1084.
[38] S.S. Zhang, D.T. Tran, J. Power Sources 211 (2012) 169–172.
[39] V.S. Kolosnitsyn, E.V. Karaseva, Russ. J. Electrochem. 44 (2008) 506–509.
[40] X.-G. Sun, X. Wang, R.T. Mayes, S. Dai, ChemSusChem 5 (2012) 2079–2085.
[41] W. Wei, J. Wang, L. Zhou, J. Yang, B. Schumann, Y. NuLi, Electrochem. Commun. 13 (2011) 399–402.
[42] J. Shim, K.A. Striebel, E.J. Cairns, J. Electrochem. Soc. 149 (2002) A1321.
[43] S. Xiong, K. Xie, Y. Diao, X. Hong, J. Power Sources 236 (2013) 181–187.
[44] Y. Diao, K. Xie, S. Xiong, X. Hong, J. Power Sources 235 (2013) 181–186.